Available online at www.sciencedirect.com

ScienceDirect

journal homepage: www.keaipublishing.com/jtte

Original Research Paper

Simulating bicycle traffic by the intelligent-driver model-Reproducing the traffic-wave characteristics observed in a bicycle-following experiment

Valentina Kurtc [a,*], *Martin Treiber* [b]

[a] *Institute of Applied Mathematics and Mechanics, Peter the Great St. Petersburg Polytechnic University, St. Petersburg 195251, Russia*

[b] *Institute for Transport and Economics, Technische Universität Dresden, Dresden 01062, Germany*

HIGHLIGHTS

- The intelligent-driver model (IDM) can describe "bicycle-following" traffic.
- Generally, the IDM trajectories fit even better to the data than that of the necessary deceleration model (NDM).
- The IDM calibration is more robust in comparison to the NDM.
- Validation results show that the IDM predictive power is better than that of the NDM.
- For bicycle traffic inter-driver variation is higher than the intra-driver variation.

ARTICLE INFO

Article history:
Received 31 August 2018
Received in revised form
17 March 2019
Accepted 19 March 2019
Available online 3 January 2020

Keywords:
Bicycle traffic
Car-following model
Stop-and-go waves
Calibration
Validation
Fundamental diagram

ABSTRACT

Bicycle traffic operations become increasingly important and yet are largely ignored in the traffic flow community, until recently. We hypothesize that there is no qualitative difference between vehicular and bicycle traffic flow dynamics in single-file case, so the latter can be described by reparameterized car-following models. To test this proposition, we reproduce German (Andresen et al., 2014) and Chinese (Jiang et al., 2016) bicycle experiments on a ring with the intelligent-driver model (IDM) and compare its fit quality (calibration) and predictive power (validation) with that of the necessary-deceleration-model (NDM), which is specifically designed for bike traffic. We find similar quality metrics for both models, so the above hypothesis of a qualitative equivalence cannot be rejected. Moreover, calibration errors of the IDM turn up to be slightly smaller compared to the NDM ones. The NDM represents significant calibration errors for high flow densities, which correspond to flow states, when stop-and-go wave emerge. According to validation tests, the IDM outperforms the NDM as well. Performing two types of validation techniques we discover that inter-driver variation is much higher than the intra-driver variation for bicycle traffic. It coincides with the results obtained from vehicular traffic experiments (NGSIM trajectory data). In addition, we suggest the measure for quantitative comparison of two microscopic fundamental diagrams, which are derived from experimental data and

* *Corresponding author*. Tel.: +7 921 632 5856.
E-mail addresses: kurtsvv@gmail.com (V. Kurtc), martin.treiber@tu-dresden.de (M. Treiber).

Peer review under responsibility of Periodical Offices of Chang'an University.
https://doi.org/10.1016/j.jtte.2019.03.005

simulated trajectories. The analysis of speed-density relations provides more or less the same results for both models.

1. Introduction

Nowadays pollution and serious congestions lead to a gradual increase of bicycle trips (Pucher and Buehler, 2008). Some studies were conducted which proved the health benefits of individuals changing from private car to cycling (Doorley et al., 2017; Mueller et al., 2015). As a result, studies of bicycle flow are important for design and operation of bicycle facilities. In spite of its growing relevance, past research on bicycle traffic operations in experiments (Jiang et al., 2016; Navin, 1994; Taylor and Davis, 1999; Zhang et al., 2014) and models (Andresen et al., 2014; Gould and Karner, 2009; Jia et al., 2007; Jiang et al., 2004; Jin et al., 2015; Li et al., 2008, 2009; Vasic and Ruskin, 2012; Zhang et al., 2013; Zhao et al., 2009, 2013) is remarkably scarce. In contrast, there is a multitude of empirical and experimental investigations for vehicular traffic flow, as well as a plethora of models (Chowdhury et al., 2000; Kerner, 2009, 2013; Nagel et al., 2003; Treiber and Kesting, 2013) and for pedestrian flows (Blue and Adler, 2001; Helbing et al., 2005; Hoogendoorn and Daamen, 2005; Seyfried et al., 2009). Therefore, it is natural to ask whether there is a significant qualitative difference between vehicular and bicycle traffic flow at all. In other words, the question arises if one can use the well-developed car-following models for the simulation of bicycle traffic instead of creating new bicycle models.

In this paper, we test the intelligent driver models (IDM) (Treiber and Helbing, 1999; Treiber et al., 2000) as a typical representative of car-following models against the "ring-road" bicycle traffic experiments (Andresen et al., 2014; Jiang et al., 2016; Zhang et al., 2014). In addition, we compare the IDM fit quality with that of a specifically designed "bicycle-following model", the necessary deceleration model (NDM) (Andresen et al., 2014). The NDM is the only "car-following model" applied to simulate bicycle traffic flow, to date. Moreover, the authors of this model state, that they developed the NDM as a car-following-model to investigate driving behavior of cyclists (Andresen et al., 2014).

In the following two sections, we shortly describe the models and the experiments. Section 4 specifies the calibration procedure before we present our main calibration and validation results in Section 5 and conclude with a discussion in Section 6.

2. Models under investigation

Two microscopic car-following models are considered – the IDM (Treiber and Helbing, 1999; Treiber et al., 2000) and the NDM (Andresen et al., 2014). Both of them are formulated as a set of coupled ordinary differential equations and are characterized by an acceleration function which depends on the actual speed $v(t)$, the approaching rate $\Delta v(t) = v(t) - v_L(t)$ to the leader (v_L is the leading vehicle speed), and the gap $s(t)$.

The IDM is defined by the acceleration function (Treiber et al., 2000) as

$$\dot{v}_{IDM}(v, \Delta v, s) = a\left[1 - \left(\frac{v}{v_0}\right)^4 - \left(\frac{s^*(v, \Delta v)}{s}\right)^2\right] \tag{1}$$

where s is the actual (bumper-to-bumper) gap and $s^*(v, \Delta v) = s_0 + \max(0, vT + v\Delta v/(2\sqrt{ab}))$ is the dynamically desired gap. The IDM contains five parameters to identify via calibration, a, v_0, s_0, T and b. Recently, it has been found that stochasticity plays a significant role for low-speed traffic flow, so we have added the simplest form of white acceleration noise to the acceleration equation (Treiber and Kesting, 2017) when simulating collective effects.

The NDM is originally formulated in terms of difference equations for the speed (Andresen et al., 2014) which, in the limit of update times Δt tending to zero, is equivalent to a coupled differential equation with the acceleration function as

$$\dot{v}_{NDM}(v, \Delta v, s) = \mathrm{acc} - \min(\mathrm{dec}_1 + \mathrm{dec}_2, b_{max}) \tag{2}$$

where b_{max} is the maximum braking deceleration and

$$\mathrm{acc} = \begin{cases} 0 & s \le d(v) \\ \dfrac{v_0 - v}{\tau} & s > d(v) \end{cases} \tag{3}$$

$$\mathrm{dec}_1 = \begin{cases} \min\left(\dfrac{(\Delta v)^2}{2(s - l - s_0)}, b_{max}\right) & \Delta v < 0 \\ 0 & \text{otherwise} \end{cases} \tag{4}$$

$$\mathrm{dec}_2 = \begin{cases} b_{max}\dfrac{(s - d(v))^2}{(l - d(v))^2} & s \le d(v),\ \Delta v \ge -\epsilon \\ 0 & \text{otherwise} \end{cases} \tag{5}$$

The safety distance $d(v) = s_0 + l + vT$ is a linear function of the cyclist's speed v, l is a length of the bicycle, ϵ is a small positive constant parameter, which is equal to 0.5 m/s. As the IDM, the NDM has 5 parameters to calibrate, τ, v_0, s_0, T and b_{max}.

3. Ring-road experiment

Trajectory data of two independent sets of bicycle experiments were considered for calibration and validation. The first set of experiments was conducted by the University of Wuppertal in cooperation with Julich Forschungszentrum on 6th of

May, 2012 (Andresen et al., 2014). Cyclists aged 7–66 years old were moving one after another along the oval track of 86 m length. However the measuring area covered only a straight line of 20 m length. Group experiments were performed for several density levels, 5, 7, 10, 18, 20 and 33 participants. Cyclists were told to drive normally without overtaking. Two cameras overlooked the whole area, so all trajectories of cyclists were captured and extracted.

Another set of experiments has been performed with 39, 48 and 63 cyclists (Jiang et al., 2016). It was conducted three times accounting for different weather conditions (sunny, sunny/cloudy and a little rainy) and both male and female riders participated. The geometry of the track was an oval with 29 m long straight sections joined by two semi-circular curves of radius 14 m resulting in a circumference of 146 m. The number of cyclists was different in the three runs to reproduce different global densities, similarly to the experimental protocol of the vehicle flow experiments of Sugiyama et al. (2008) and the pedestrian flow experiments of Helbing et al. (2005) and Seyfried et al. (2005). The riders were filmed by one video camera mounted on the top of an 18-story building, so, in contrast to the German experiments, the complete trajectories could be obtained. Furthermore, the trajectories cover a longer time interval compared to the experiments of Andresen et al. (2014). The experiments by Jiang et al. (2016) gave essentially the same results as the German experiments and demonstrated even more pronounced stop-and-go waves for the higher densities.

4. Methods

We have estimated the model performance by two approaches. One is based on trajectories, and the other on aggregated properties of scatter plots derived from stationary measurements (virtual detectors).

4.1. *Data pre-processing*

First, the directly recorded two-dimensional positional data x and y are transformed into arc-lengths z using the geometry of the closed test tracks (Fig. 1). In Fig. 1, the global densities on the closed track of 146 m length were 0.267, 0.329, and 0.432 m^{-1}, respectively. The color coding repeats after every 10th cyclist. Since the original data contained a significant amount of noise due to measurement and rounding errors (rounded to multiples of 0.1 or even 0.5 m) and the noise is aggravated when deriving the speed, a smoothing procedure is necessary. For this purpose, we have applied exponential smoothing of the arc-length data with a symmetric exponential kernel $w(t) \propto \exp(|t|/\tau)$ as a function of time difference t, assuming a smoothing width $\tau = 0.2$ s. Other values for τ did not produce significantly different calibration results. The speeds have been obtained from the smoothed arc-length data by symmetric finite differences. Specifically, the speed v_i^k of cyclist i at time $t = k\Delta t$ has been calculated by

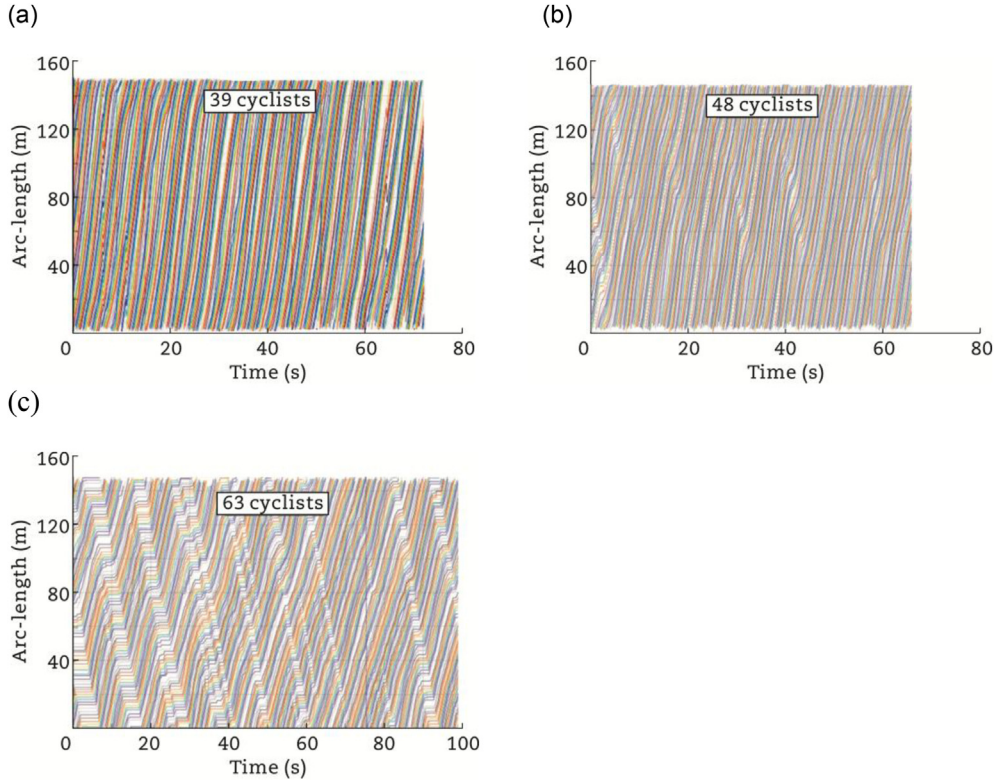

Fig. 1 – Trajectory data of the three experiments of Jiang et al. (2016) after the warm-up phase. (a) 39 cyclists. (b) 48 cyclists. (c) 63 cyclists.

$$v_i^k = \frac{z_i^{k+1} - z_i^{k-1}}{2\Delta t} \tag{6}$$

where the sampling interval $\Delta t = 1/f$ with $f = 10$ Hz or $f = 15$ Hz depends on the data set, and z_i^k is the monotonously increasing "unrolled" arc-length coordinate of cyclist i at time $t = k\Delta t$ such that the coordinate of the leader is always greater than that of the follower.

Notice that, when calculating the speed, we did not apply further smoothing in order to conserve the local and platoon consistency of the data (Montanino and Punzo, 2013; Punzo et al., 2011; Treiber and Helbing, 2013).

4.2. *Calibrating and validating trajectories*

Pairs of consecutive trajectories were used for calibration and validation according to the global approach (Kurtc and Treiber, 2016; Treiber and Kesting, 2013). Specifically, the simulated speed v^{sim} of the microscopic model was initialized with the empirically given speed v^{data}, and likewise for the gaps, $v^{\text{sim}}(t=0) = v^{\text{data}}(t=0)$ and gap $s^{\text{sim}}(t=0) = s^{\text{data}}(t=0)$, and the trajectory of the following cyclist for a given leader trajectory was calculated using the ballistic update (Chapter 10.2 of Treiber and Kesting (2013)). Afterward, the simulated gaps $s^{\text{sim}}(t)$ were compared with the experimentally observed gaps $s^{\text{data}}(t)$ by means of two objective functions, namely the absolute error measure (Eq. (7)) and the relative error measure (Eq. (8)).

$$s^{\text{abs}} = \frac{\sum_{i=1}^{n} \left(s_i^{\text{sim}} - s_i^{\text{data}}\right)^2}{\sum_{i=1}^{n} \left(s_i^{\text{data}}\right)^2} \tag{7}$$

$$s^{\text{rel}} = \frac{1}{n} \sum_{i=1}^{n} \left(\frac{s_i^{\text{sim}} - s_i^{\text{data}}}{s_i^{\text{data}}} \right)^2 \tag{8}$$

We also calibrated according to the mixed error as defined in Chapter 16 of Treiber and Kesting (2013), and found no significant differences.

In the experiment of Andresen et al. (2014), the trajectories have been recorded for only a 20-m section of the circumference of 86 m, while the complete circumference of 146 m has been recorded for the Chinese experiments. This also means that a single trajectory pair has been split into several pairs in the experiment of Andresen et al., while, in the Chinese experiment, all 39, 48, or 63 trajectory pairs include the complete duration of the experiment, excluding only the warm-up phase.

4.3. *Comparing microscopic fundamental diagrams*

We used virtual stationary detectors at several positions of the ring and calculated.

- The instantaneous speed v_i of cyclist i at passage time,
- The "microscopic density" ρ_i, i.e., the inverse space headway to the leader at passage time,
- The microscopic flow $Q_i = \rho_i v_i$, i.e., the inverse (time) headway.

We combined these data to microscopic speed-density scatter plots both for the simulations and the experiments by defining the sets $[\rho_i^{\text{data}}, v_i^{\text{data}}]$ and $[\rho_i^{\text{model}}, v_i^{\text{model}}]$, respectively. In order to quantitatively compare the similarity, we create a partitioning of the data points by filtering them according to N equally-spaced density intervals,

$$V_j^{\text{src}} = \left\{ v_i^{\text{src}} : \rho_i^{\text{src}} \in \left[\rho_j, \rho_{j+1}\right], i = 1, \cdots, M_{\text{src}} \right\} \tag{9}$$

where $j = 1, \cdots, N$, src $= \{\text{data, model}\}$. The key idea is to interpret V_j^{src} as a one-dimensional random variable. Now we calculate the (cumulative) distribution functions both for the experiment, $F_{V_j^{\text{data}}}(x)$, and the simulations, $F_{V_j^{\text{model}}}(x)$, and calculate the Kolmogorov–Smirnov distance as

$$D_j = \sup_x \left| F_{V_j^{\text{data}}}(x) - F_{V_j^{\text{model}}}(x) \right| \quad j = 1, \cdots, N \tag{10}$$

The distance D_j is averaged over all density bins giving D^* and provides the quantitative metric which estimates the similarity of two data-clouds

$$D^* = \frac{1}{N} \sum_{j=1}^{N} D_j \tag{11}$$

5. Results

5.1. *Free acceleration*

First, we compare and calibrate the free acceleration profile against the experimental results. After calibrating the relevant IDM parameters to the values $v_0 = 4.3$ m/s and $a = 1.0$ m/s^2 and adding a small amount of white noise (intensity $Q = 0.02$ m^2/s^3) the IDM could reproduce the acceleration profile better than the NDM (Fig. 2). This figure displays a typical experimental profile and the NDM prediction taken from Andresen et al. (2014) experiment and two realizations from the stochastic IDM.

5.2. *Collective driving behavior*

We will now calibrate the NDM and the IDM on all the leader–follower pairs of the Chinese experiments of Jiang et al. (2016).

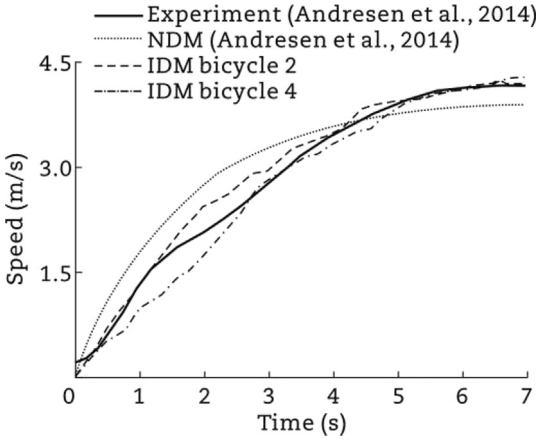

Fig. 2 – First stage of the free acceleration of cyclists.

The first five panels of Fig. 3 display the cumulative distribution functions (CDFs) of the calibrated NDM parameters for the experiments with 39, 48, and 63 bikers corresponding to a global density $\rho = 0.267$ m^{-1}, $\rho = 0.329$ m^{-1}, and $\rho = 0.432$ m^{-1}, respectively. Generally, we observe a wide scattering of the calibrated parameters. Since the degree of fitting is comparatively high (more than 70% of the trajectory pairs of the first two experiments result in an absolute error measure $S^{abs} < 0.1$), we can conclude that the intra-driver variations (whose upper limit is characterized by the error measure) are generally lower than the inter-driver variations which are characterized by the spread of the relevant parameters. Notice that, at the highest density, the NDM (and the IDM) parameter v_0 becomes irrelevant since it characterizes free flow.

Fig. 4 displays the calibration results to the same data for the IDM. Generally, the IDM fitting quality is slightly better with more than 90% of all trajectory pairs of the first two experiments having an error measure $S^{abs} < 0.1$. Interestingly, the IDM is better suited to describe the high-density data and the associated stop-and-go waves while the NDM fares best at the runs with the lower densities (which, nevertheless, correspond to rather crowded situations).

Finally, we observe that distinct and persistent inter-driver variations can also be observed directly in the trajectory data (Fig. 1). For example, the driver corresponding to the black trajectory crossing $z = 0$ at about $t = 14$ s keeps consistently much more space to his or her leader compared to most of the other cyclists. In both the IDM and the NDM, this corresponds to high values of s_0 and/or T for this driver.

Table 1 presents the calibration errors of both German and Chinese experiments. For both error measures (Eqs. (7) and (8))

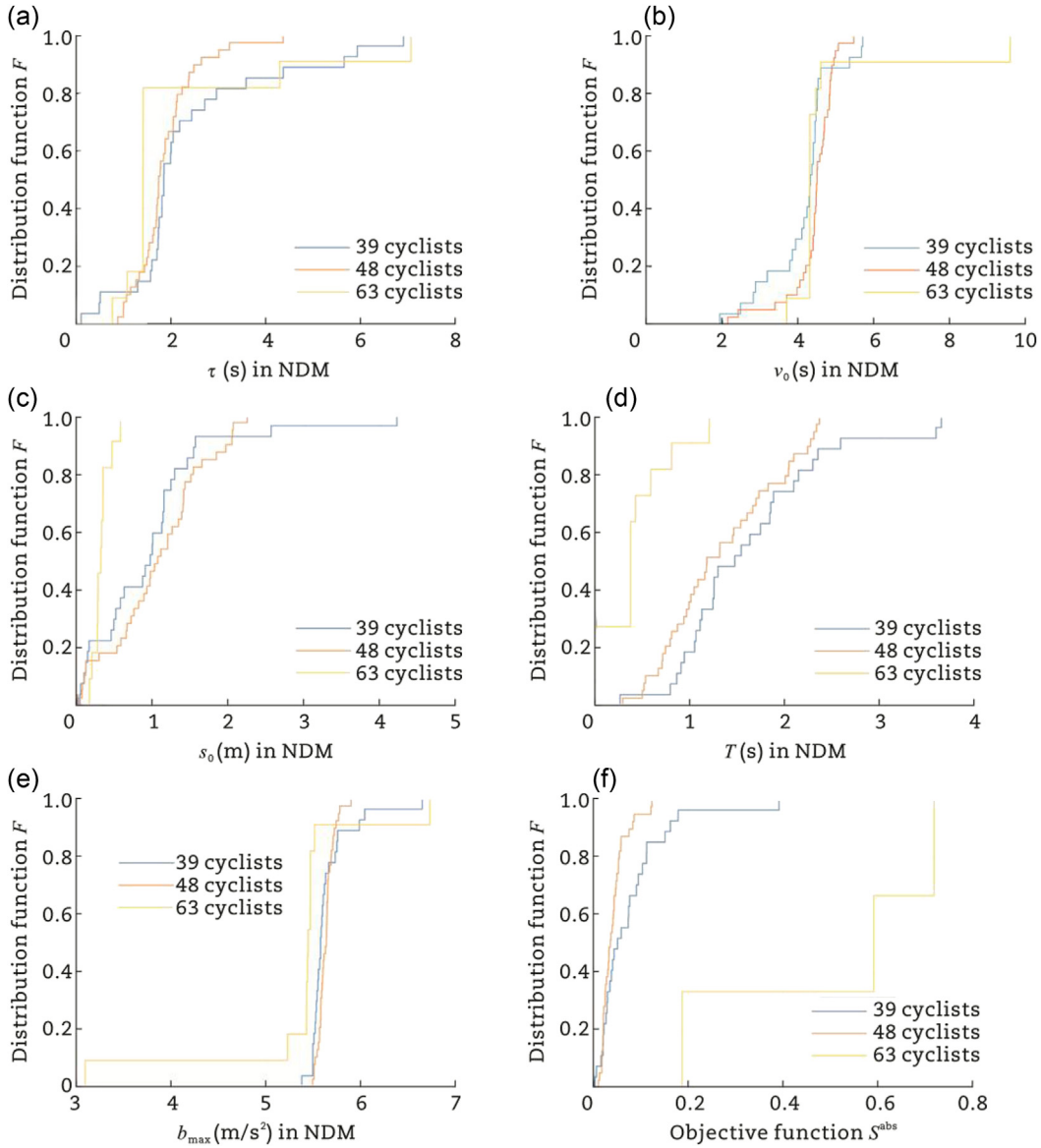

Fig. 3 – Cumulative distribution functions for the NDM parameters as obtained from the calibration of all 39, 48, and 63 cyclists of the corresponding experiments of Jiang et al. (2016). (a) τ. (b) v_0. (c) s_0. (d) T. (e) b_{max}. (f) Associated objective function S^{sbs}.

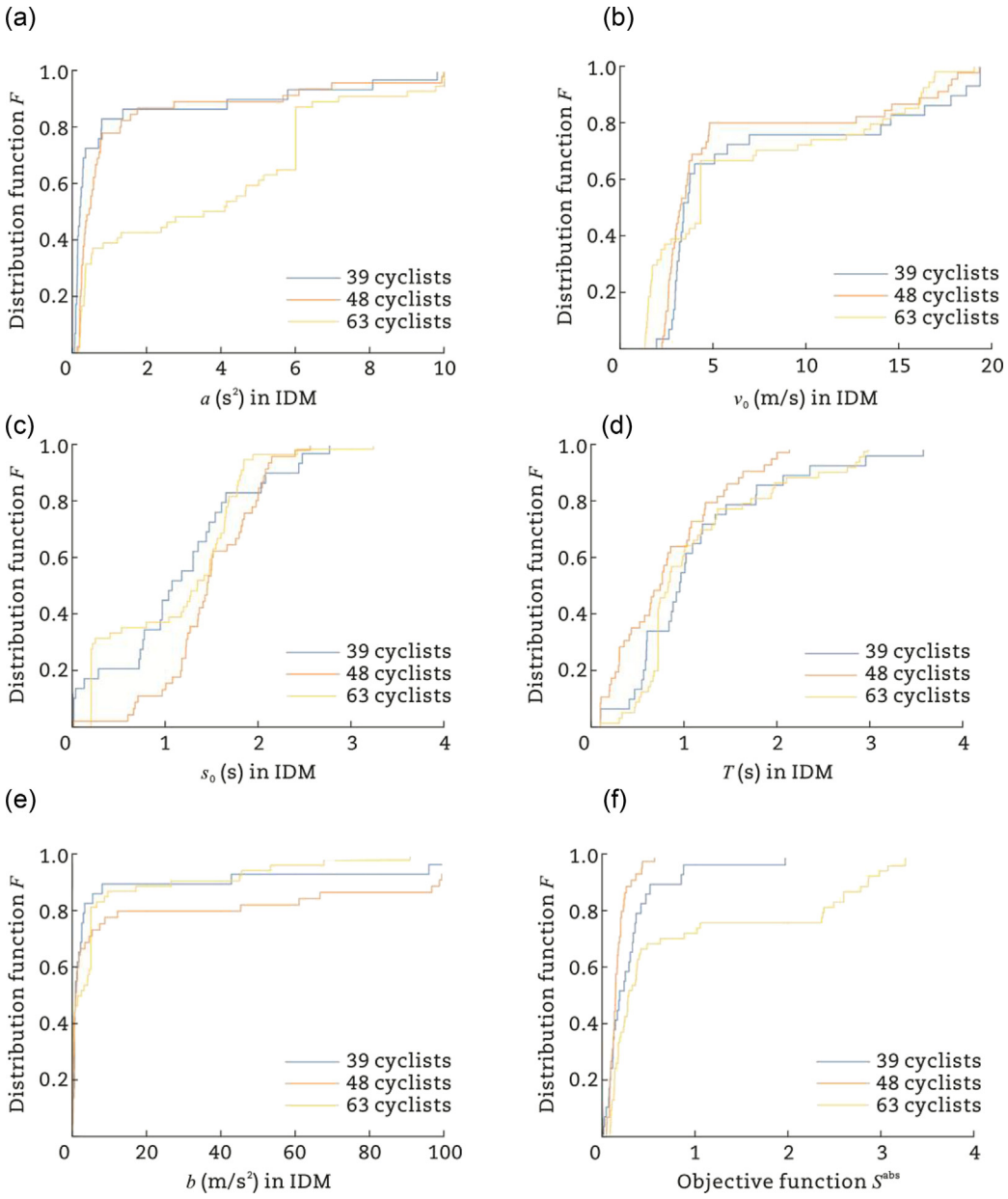

Fig. 4 – Cumulative distribution functions for the IDM parameters as obtained from the calibration of all 39, 48, and 63 cyclists of the corresponding experiments of Jiang et al. (2016). (a) *a*. (b) v_0. (c) s_0. (d) *T*. (e) *b*. (f) Associated objective function S^{abs}.

and experiments of Andresen et al. (2014) lower error values correspond to the IDM whereas higher errors come from the NDM. As for experiments of Jiang et al. (2016) the error values are nearly the same.

The use of several error measures can be interpreted as a benchmark for the robustness of the model calibration. Specifically, for a good model, the calibration results and the distribution of the calibrated parameters should not significantly vary with the chosen error measure. We compare the Kolmogorov–Smirnov distance (Eq. (12)) of the distributions $F_{1,n}$ and $F_{2,n}$ of parameter n as obtained by calibrating the trajectories with respect to the absolute and relative error measure S^{abs} and S^{rel}, respectively. According to the results presented in Table 2, the IDM tends to be slightly more robust than the NDM. However results in Table 3 indicate that both models are more or less equivalent in this context.

Table 1 – Calibration errors (%) for IDM and NDM (averaged over all trajectories).

Model	Andresen et al. (2014)		Jiang et al. (2016)	
	$\sqrt{S^{abs}}$	$\sqrt{S^{rel}}$	$\sqrt{S^{abs}}$	$\sqrt{S^{rel}}$
IDM	1.92	1.95	25.64	24.85
NDM	4.53	4.58	23.40	23.30

Table 2 – Kolmogorov–Smirnov distance Eq. (12) D_n of the parameter values for the two models (Andresen et al., 2014).

Parameter	IDM					NDM				
	D_a	D_{v_0}	D_{s_0}	D_T	D_b	D_τ	D_{v_0}	D_{s_0}	D_T	$D_{b_{max}}$
Value	0.027	0.033	0.036	0.056	0.027	0.065	0.042	0.050	0.051	0.052

$$D_n = \sup_x \left| F_{1,n}(x) - F_{2,n}(x) \right| \tag{12}$$

5.3. *Microscopic fundamental diagrams comparison*

We have calculated the microscopic fundamental diagram and the distance measures both for the real data and for the simulation of the two models with the optimal parameter values without noise. The results are shown in Fig. 5.

5.4. *Reproducing stop-and-go waves by the IDM*

Besides calibrating the IDM by trajectory pair, we also tested if the IDM can produce collective effects such as the stop-and-go traffic observed in the experiments of Andresen et al. (2014) and Jiang et al. (2016). Fig. 6 shows the result. Instead of using heterogeneous drivers, we simplified the investigation as much as possible by using a single parameter set for all drivers replacing the heterogeneity by white acceleration noise. In contrast to the free-flow simulation (Fig. 3), a higher amount of 0.1 m^2/s^3 was needed to approximatively reproduce the observed amplitude and frequency statistics of the traffic waves while the free-flow parameters $v_0 = 4.3$ m/s and $a = 1.0$ m/s^2 were the same. The calibrated values $T = 0.85$ s, $s_0 = 0.4$ m, and $b = 1.3$ m/s^2 were near the median of the trajectory-by-trajectory calibration of Section 5.2.

5.5. *Inter-driver variation and validation*

Validation by cross comparison implies determining the error measures for a certain test data set by simulating the model with the parameters calibrated to the disjunct "learning" data set (Treiber and Kesting, 2013). For each experiment (5, 10, 15, 18, 20 and 33 cyclists, respectively), we have separately calculated the calibration-validation matrix whose elements M_{ij} give the error measure $\sqrt{S^{abs}}$ for the trajectory pair j as obtained from the model calibrated to the trajectory pair i. The diagonal element M_{ii} is the calibration errors whereas the off-diagonal elements $M_{ji}(j \neq i)$ give a superposition of the validation error and the inter-driver variation of follower j with respect to follower i. The average validation error ϵ^{val} and calibration error ϵ^{cal} are given by

$$\epsilon^{val} = \frac{1}{n(n-1)} \sum_{i=1}^{n} \sum_{\substack{j=1 \\ j \neq i}}^{n} M_{ij} \tag{13}$$

$$\epsilon^{cal} = \frac{1}{n} \sum_{i=1}^{n} M_{ii} \tag{14}$$

where n is a number of trajectory pairs. To obtain measures for the overall fitting quality and the predictive power plus inter-driver variations, we have calculated the ratio of the average validation error to the calibration error (Table 4).

In order to separate the validation error and the inter-driver variation we used disjunct parts of the same trajectory for calibration and validation. Trajectories from Jiang et al. (2016) experiments are quite long, what allows performing holdout validation. The first half of each trajectory was selected for calibration, whereas the second half was used for validation. Table 5 represents fitting power (calibration error) and predictive power (validation error) as well as the ratio between these two measures for each experiment (39, 48 and 63 cyclists) and both models (IDM and NDM).

Calibration errors more than 100% and validation errors more than 1000% were interpreted as outliers and were filtered out (Tables 4 and 5).

6. Discussion and conclusions

The traffic flow dynamics of bicycles has been ignored for many years, and this paper is the first to quantitatively compare two models on two sets of data. Moreover, it has shown, to our knowledge for the first time, that certain microscopic models devised for cars (car-following models, particularly the IDM) also can describe bicycle-following traffic at least as well as dedicated models.

Bicycle driving typically is not lane based (although there are bike paths with lanes on some US campuses). Bicycle drivers are much more flexible than car drivers and often overtake each other, even if there is relatively little space. Moreover, multi-lane bike paths are rare while, particularly in countries such as Holland, they are wide allowing for two or

Table 3 – Kolmogorov–Smirnov distance Eq. (12) D_n of the parameter values for the two models (Jiang et al., 2016).

Parameter	IDM					NDM				
	D_a	D_{v_0}	D_{s_0}	D_T	D_b	D_τ	D_{v_0}	D_{s_0}	D_T	$D_{b_{max}}$
N = 39	0.17	0.10	0.17	0.33	0.16	0.15	0.26	0.15	0.30	0.15
N = 48	0.16	0.10	0.11	0.16	0.13	0.17	0.18	0.18	0.23	0.14
N = 63	0.11	0.13	0.20	0.07	0.09	0.32	0.19	0.20	0.18	0.20

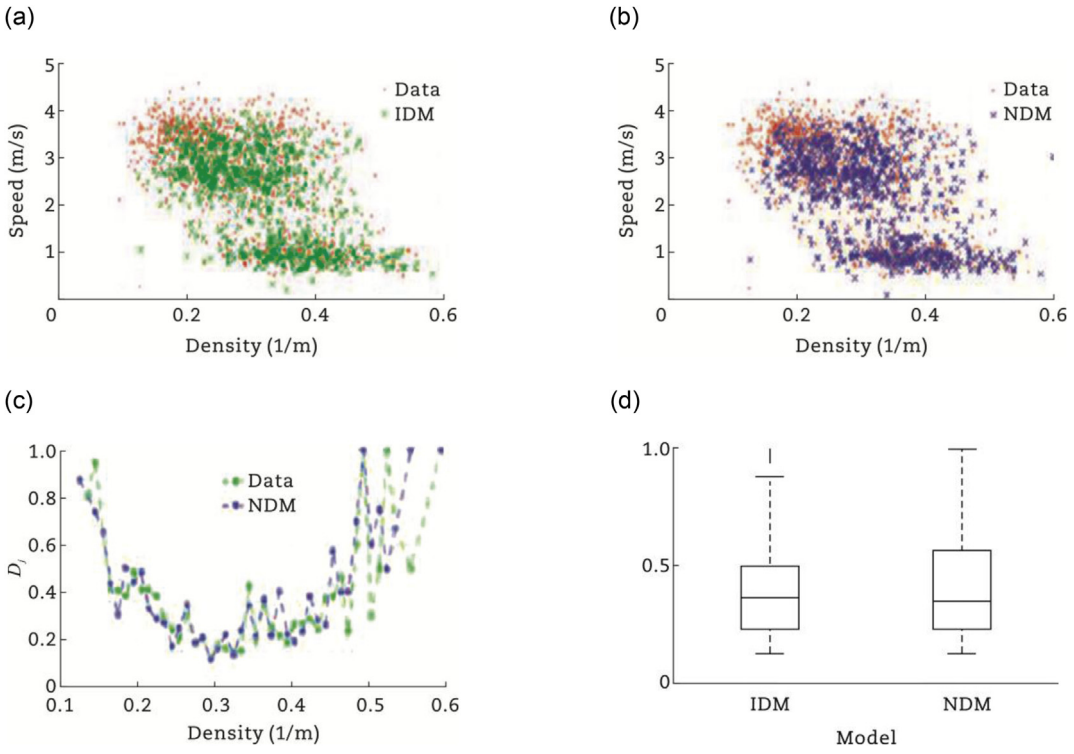

Fig. 5 – Speed-density relation for the data. (a) IDM. (b) NDM. (c) Values of the metric D_j for jth density bin. (d) Boxplots corresponding to the IDM (left) and the NDM (right).

even three cyclists driving in parallel which clearly demands for a true 2d model to couple longitudinal and lateral dynamics such as the social-force model for pedestrians. However, adhering to the scientific approach to isolate aspects as far as possible, this paper concentrates exclusively on the longitudinal dynamics. Since there are no data for bicycle drivers driving "not" in single file, it also makes no sense to develop and simulate 2d models at this stage. Nevertheless, a fully 2d continuous IDM for non-lane-based mixed two-wheeler and four-wheeler traffic, which is encountered often in some countries, e.g., in India, has been developed (Kanagaraj and Treiber, 2018).

According to the results presented in this paper, we conclude that the IDM, which has a similar underlying heuristics as the NDM, can not only describe vehicular but also bicycle-following traffic. Generally, the IDM trajectories fit even better to the data than that of the NDM. For the German experiments conducted by Andresen et al. (2014), we obtain, on average, absolute and relative IDM error measures of 1.92% and 1.95% while that for the NDM are 4.53% and 4.58%, respectively. This is confirmed by applying the models to the Chinese experiments of Jiang et al. (2016) resulting for the IDM in absolute and relative errors of 25.64% and 24.85% while, for the NDM, we obtained 23.40% and 23.30% with the highest errors for the highest density (Table 5). Since this is also the density, where most stop-and-go waves are observed, there is evidence that the IDM is

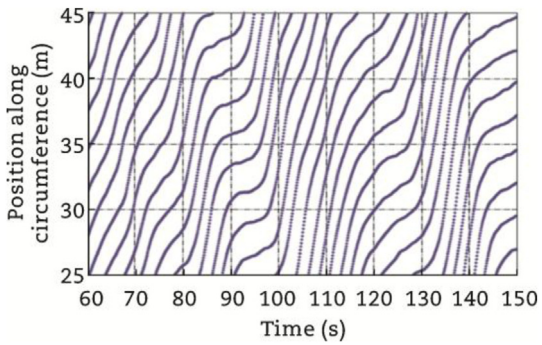

Fig. 6 – Simulated trajectories of stop-and-go traffic appearing for the IDM for dense traffic (density 300 cyclists/km).

Table 4 – Calibration, validation errors (%) and averaged ratios for IDM and NDM (Andresen et al., 2014).

Cyclists	$N = 5$	$N = 10$	$N = 15$	$N = 18$	$N = 20$	$N = 33$
IDM						
Calibration error	0.78	0.98	1.11	1.11	1.34	3.43
Validation error	28.70	28.81	28.60	32.55	31.66	43.29
Ratio	36.90	29.50	25.80	16.00	23.60	12.60
NDM						
Calibration error	1.65	2.27	3.59	3.94	4.78	6.75
Validation error	33.57	24.55	27.82	30.35	28.75	30.74
Ratio	20.40	10.80	7.70	7.70	6.00	4.50

Table 5 – Calibration and holdout validation errors (%) and averaged ratios for IDM and NDM (Jiang et al., 2016).

Cyclists	$N = 39$	$N = 48$	$N = 63$
IDM			
Calibration error	18.27	15.43	32.15
Validation error	26.71	22.18	34.13
Ratio	1.50	1.40	1.10
NDM			
Calibration error	23.83	18.75	62.95
Validation error	28.11	21.77	58.35
Ratio	1.20	1.20	0.90

particularly suited to describe highly dynamical situations such as stop-and-go traffic.

The different error levels (Table 1) stem from the different lengths of the trajectories. Since these cover less than 20 m in the German experiment and often there are no significant accelerations during this time, it is very easy to calibrate and lead to unrealistically low errors of a few percent, only. In contrast, the Chinese trajectory pairs include several stop-and-go phases (Fig. 1) which makes them harder to calibrate. The approx 20% error levels of the IDM and the NDM in the Chinese experiments can be considered as good; they are on the same level as the calibration errors of vehicular trajectory pairs (Brockfeld et al., 2005). Finally, we should highlight, that the short trajectory data of the German experiment are not really useful for calibration and validation.

The application of several objective functions indicates that the IDM calibration is also more robust in comparison to the NDM. Validation results show that the predictive power of the NDM is better than that of the IDM. The validation results from Andresen et al. (2014) experiment are superposition of the validation error and the inter-driver variation. The ratio of this all-inclusive validation error to the calibration error is in range from 12.6 to 36.9 for IDM and from 4.5 to 20.4 for NDM. Trajectories from Jiang et al. (2016) experiment are longer, which enabled hold-out validation. This method allows excluding inter-driver variation from validation error. As a result, ratios are significantly lower: 1.1–1.5 for IDM and 0.9–1.2 for NDM. One can conclude that for bicycle traffic inter-driver variation is higher than the intra-driver variation is. The same results were obtained for vehicular traffic (Kurtc and Treiber, 2016).

The analysis of macroscopic characteristics such as speed-density relations provides more or less the same results for both models. Fundamental diagrams (Fig. 5) of both models do not deviate significantly from the experimental results. However one can say that experimental data are slightly more scattered for low density values. What is interesting, that speed-density relations for the data and both models represent two distinct data clouds, which can be interpreted as two different states, free flow and congested flow as it is in traffic flow theory. The averaged Kolmogorov distance D^* (Eq. (11)) is nearly the same. Furthermore, the stochastic IDM can well describe the statistical features of the amplitude and frequency of the observed stop-and-go waves.

It is one of the remarkable results of this paper that the difference seems to be of a quantitative rather than qualitative nature. Otherwise, the dedicated bicycle model would have a better calibration/validation performance. This can be explained by the fact that both the bike and the motorized car (or motorbike) driver have a desired or maximum speed, a preferred time gap in following mode, a certain minimum gap in stopped traffic, and preferred (and maximum) accelerations and decelerations, so any model encompassing these attributes (such as the IDM) should be able to describe both motorized and non-motorized traffic. Basically, the intuitive meaning of the IDM parameters carries over to bicycle traffic. While, obviously, the desired speed is lower, the parameters T and s_0 still have the meaning of a preferred time gap and minimum gap, respectively. Remarkably, the time–gap parameter T is not so different from that observed in car-following experiments, while it is somewhat lower than that observed in naturalistic car-driving data. Furthermore, the desired (comfortable) deceleration and maximum acceleration are of the same order as for car traffic. The similarities of the parameters T, a, and b reflect similar physiological constraints (the human reaction time for T) and physical constraints: the maximum braking deceleration for cars and bikes is of the same order, about a safety factor of 5 higher than the comfortable deceleration. Also the low-speed maximum acceleration is comparable: when starting at a traffic light turning green, cars are only faster than bikers after 10–15 m, or so.

We conclude that the dynamics of bicycle traffic differs only quantitatively from vehicular traffic and reparameterized car-following models such as the IDM work at least as well as dedicated "bike-following" models. No qualitative difference between vehicular and bicycle traffic flow dynamics for the case of single-lane traffic was found. There is free traffic, congested traffic, traffic flow instabilities with backwards propagating traffic waves, qualitatively the same fundamental diagram and all that. The fact that there is a "quantitative" differences, e.g., maximum speeds of 120 vs 20 km/h and different vehicle sizes does not make the difference qualitative. The longitudinal dynamics of cyclists and car drivers is governed by the same objectives (desired speed, desired time gap, minimum gap) and the same limits (reaction time, acceleration, and deceleration). One may argue that one qualitative difference, in fact, exists: a biker (whether cyclist or motorcyclist) cannot drive very slowly because then they would fall from their bike unless being an artist. However, driving a car very slowly is also cumbersome, particularly one with manual transmission where the clutch needs to be operated all the time. In practice, this does not make a significant difference.

Conflict of interest

The authors do not have any conflict of interest with other entities or researchers.

Acknowledgments

We would like to thank Erik Andresen and Dr. Rui Jiang for the provision of experimental data.

REFERENCES

Andresen, E., Chraibi, M., Seyfried, A., et al., 2014. Basic driving dynamics of cyclists. In: Simulation of Urban Mobility, Berlin, 2014.

Blue, V.J., Adler, J.L., 2001. Cellular automata microsimulation for modeling bi-directional pedestrian walkways. Transportation Research Part B: Methodological 35 (3), 293–312.

Brockfeld, E., Kuhne, R.D., Wagner, P., 2005. Calibration and validation of microscopic traffic flow models. Transportation Research Record 1934, 62–70.

Chowdhury, D., Santen, L., Schadschneider, A., 2000. Statistical physics of vehicular traffic and some related systems. Physics Reports 329 (4–6), 199–329.

Doorley, R., Pakrashi, V., Ghosh, B., 2017. Health impacts of cycling in Dublin on individual cyclists and on the local population. Journal of Transport & Health 6, 420–432.

Gould, G., Karner, A., 2009. Modeling bicycle facility operation: cellular automaton approach. Transportation Research Record 2140, 157–164.

Helbing, D., Buzna, L., Johansson, A., et al., 2005. Self-organized pedestrian crowd dynamics: experiments, simulations, and design solutions. Transportation Science 39 (1), 1–24.

Hoogendoorn, S.P., Daamen, W., 2005. Pedestrian behavior at bottlenecks. Transportation Science 39 (2), 147–159.

Jia, B., Li, X.G., Jiang, R., et al., 2007. Multi-value cellular automata model for mixed bicycle flow. The European Physical Journal B 56 (3), 247–252.

Jiang, R., Hu, M.B., Wu, Q.S., et al., 2016. Traffic dynamics of bicycle flow: experiment and modeling. Transportation Science 51 (3), 791–1029.

Jiang, R., Jia, B., Wu, Q.S., 2004. Stochastic multi-value cellular automata models for bicycle flow. Journal of Physics A: Mathematical and General 37 (6), 2063–2072.

Jin, S., Qu, X., Xu, C., et al., 2015. An improved multi-value cellular automata model for heterogeneous bicycle traffic flow. Physics Letters A 379 (39), 2409–2416.

Kanagaraj, V., Treiber, M., 2018. Self-driven particle model for mixed traffic and other disordered flows. Physica A: Statistical Mechanics and its Applications 509, 1–11.

Kerner, B.S., 2009. Introduction to Modern Traffic Flow Theory and Control: the Long Road to Three-phase Traffic Theory. Springer, Berlin.

Kerner, B.S., 2013. Criticism of generally accepted fundamentals and methodologies of traffic and transportation theory: a brief review. Physica A: Statistical Mechanics and its Applications 392 (21), 5261–5282.

Kurtc, V., Treiber, M., 2016. Calibrating the local and platoon dynamics of car-following models on the reconstructed NGSIM data. Traffic and Granular Flow'15, Nootdorp, 2016.

Li, X.G., Gao, Z.Y., Jia, B., et al., 2009. Modeling the interaction between motorized vehicle and bicycle by using cellular automata model. International Journal of Modern Physics C 20 (2), 209–222.

Li, X.G., Gao, Z.Y., Zhao, X.M., et al., 2008. Multi-value cellular automata model for mixed non-motorized traffic flow. Physics of Condensed Matter 56 (3), 247–252.

Montanino, M., Punzo, V., 2013. Making NGSIM data useable for studies on traffic flow theory: multistep method for vehicle trajectory reconstruction. Transportation Research Record 2390, 99–111.

Mueller, N., Rojas-Rueda, D., Cole-Hunter, T., et al., 2015. Health impact assessment of active transportation: a systematic review. Preventive Medicine 76, 103–114.

Nagel, K., Wagner, P., Woesler, R., 2003. Still flowing: approaches to traffic flow and traffic jam modeling. Operations Research 51 (5), 681–710.

Navin, F.P.D., 1994. Bicycle traffic flow characteristics: experimental results and comparisons. ITE Journal 64 (3), 31–37.

Pucher, J., Buehler, R., 2008. Making cycling irresistible: lessons from The Netherlands, Denmark and Germany. Transport Reviews 28, 495–528.

Punzo, V., Borzacchiello, M.T., Ciuffo, B., 2011. On the assessment of vehicle trajectory data accuracy and application to the Next Generation SIMulation (NGSIM) program data. Transportation Research Part C: Emerging Technologies 19 (6), 1243–1262.

Seyfried, A., Passon, O., Steffen, B., et al., 2009. New insights into pedestrian flow through bottlenecks. Transportation Science 43, 395–406.

Seyfried, A., Steffen, B., Klingsch, W., et al., 2005. The fundamental diagram of pedestrian movement revisited. Journal of Statistical Mechanics: Theory and Experiment 2005, 10002.

Sugiyama, Y., Fukui, M., Kikuchi, M., et al., 2008. Traffic jams without bottlenecks–experimental evidence for the physical mechanism of the formation of a jam. New Journal of Physics 10, 33001.

Taylor, D., Davis, W., 1999. Review of basic research in bicycle traffic science, traffic operations, and facility design. Transportation Research Record 1674, 102–110.

Treiber, M., Helbing, D., 1999. Explanation of Observed Features of Self-organization in Traffic Flow. Available at: https://arxiv.org/abs/cond-mat/9901239 (Accessed 4 December 2019).

Treiber, M., Helbing, D., 2013. An adaptive smoothing method for traffic state identification from incomplete information interface and transport dynamics. Computational Modelling 32, 343–360.

Treiber, M., Henneke, A., Helbing, D., 2000. Congested traffic states in empirical observations and microscopic simulations. Physical Review E 62, 1805–1824.

Treiber, M., Kesting, A., 2013. Traffic Flow Dynamics: Data, Models and Simulation. Springer, Berlin.

Treiber, M., Kesting, A., 2017. The intelligent driver model with stochasticity – new insights into traffic flow oscillations. Transportation Research Part B: Methodological 117, 613–623.

Vasic, J., Ruskin, H.J., 2012. Cellular automata simulation of traffic including cars and bicycles. Physica A: Statistical Mechanics and its Applications 391 (8), 2720–2729.

Zhang, J., Mehner, W., Holl, S., et al., 2014. Universal flow-density relation of single-file bicycle, pedestrian and car motion. Physics Letters A 378 (44), 3274–3277.

Zhang, S., Ren, G., Yang, R., 2013. Simulation model of speed-density characteristics for mixed bicycle flow-comparison between cellular automata model and gas dynamics model. Physica A: Statistical Mechanics and its Applications 392 (20), 5110–5118.

Zhao, X.M., Jia, B., Gao, Z.Y., et al., 2009. Traffic interactions between m-vehicles and non m-vehicles near a bus stop. Journal of Transportation Engineering 135, 894–906.

Zhao, D., Wang, W., Li, C., et al., 2013. Modeling of passing events in mixed bicycle traffic with cellular automata. Transportation Research Record 2387, 26–34.

Dr. Valentina Kurtc received the PhD degree in mathematical modeling and numerical methods from the same university, in 2017. She is an assistant professor with a permanent position at the Peter the Great St. Petersburg Polytechnic University. Dr. Kurtc is an author of more than 10 papers in peer-reviewed journals and conference proceedings in transportation field of study. Her research interests include the simulation of vehicular traffic by means on micro- and macro-approaches, calibration and validation, pedestrian dynamics.

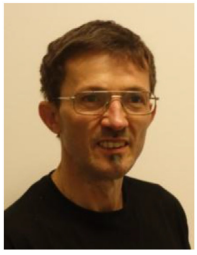

Dr. Martin Treiber is a senior research scientist with a permanent position at the Technische Universität Dresden. He obtained his PhD as a physicist at the University of Bayreuth on a macroscopic theory on traveling waves in liquid crystals. Later on, Dr. Treiber swapped waves in fluids for stop-and-go waves in congested traffic flow and moved to Dresden where he can also pursue his activities as a keen rock climber. Together with his friend and colleague Dr. Arne Kesting, he wrote two textbooks including "Traffic Flow Dynamics" (Springer Textbook XIII+503 pages, 2013). To date, he profits from his physics background and applies the numerical and mathematical methods of this field to traffic flow modeling, intelligent traffic systems, and data evaluation resulting in about 130 publications.